

# Phase retrieval for high-numerical-aperture optical systems

Bridget M. Hanser

Graduate Group in Biophysics, University of California, San Francisco, San Francisco, California 94143

Mats G. L. Gustafsson, David A. Agard, and John W. Sedat

Department of Biochemistry and Biophysics, University of California, San Francisco, San Francisco, California 94143

Received November 15, 2002

We describe a phase retrieval approach for intensity point-spread functions of high-numerical-aperture optical systems such as light microscopes. The method calculates a generalized pupil function defined on a spherical shell, using measured images at several defocus levels. The resultant pupil functions reproduce measured point-source images significantly better than does an ideal imaging model. Availability of pupil function information will facilitate new approaches to aberration correction in such systems. © 2003 Optical Society of America

OCIS codes: 100.5670, 070.2580, 180.0180, 100.0100.

Phase retrieval is a technique for estimating the wave-front properties of an imaging system from one or more intensity images, typically of a point source.<sup>1</sup> The retrieved wave-front information takes the form of a complex pupil function, which permits a more direct and quantitative analysis of an imaging system than is possible from intensity information alone. In astronomy, this technique can determine wave-front errors caused by aberrations within optical systems such as the uncorrected Hubble Space Telescope<sup>2</sup> or by atmospheric turbulence.<sup>1</sup> The retrieved wave-front information can be used to process image data<sup>3</sup> or to correct alignment of segmented mirror telescopes.<sup>4</sup>

Although they are often ignored, optical microscopy of biological specimens faces aberration problems that are similar to those in astronomy. Analogously to atmospheric turbulence, the biological sample itself can cause significant imaging aberrations that range from the depth-dependent spherical aberration caused by an overall refractive-index mismatch<sup>5</sup> to complex, spatially varying aberrations that stem from refractive-index variations within the specimen.<sup>6</sup> A method to extract wave-front information would fill a need in microscopy, as that information provides a recipe for removing aberrations by use of wave-front correction hardware<sup>7</sup> or computational approaches and because a pupil function description of the imaging system is much more easily modified to include further, known aberrations than is the conventional intensity description. Whereas phase-retrieval methods have been developed for the zero numerical aperture (NA) condition of telescopes,<sup>1–4,8–10</sup> which subtend a negligible angle as seen from the distant source, these methods must be modified to apply to high-NA conditions, such as those encountered in high-resolution microscopy. In this Letter we describe a modified phase-retrieval technique that is suitable for high-NA optical systems.

Three-dimensional (3D) imaging properties can be quantified in several ways (Fig. 1). It is common to use the 3D intensity point-spread function<sup>11</sup> (PSF)—the image of a point source as a function

of defocus, which can be directly measured—or, equivalently, the PSF's Fourier transform, the optical transfer function (OTF).<sup>12</sup> However, these descriptions are incomplete: the intensity PSF is the squared magnitude of the complex-valued amplitude (PSF<sub>A</sub>) and thus lacks the phase information of PSF<sub>A</sub>.

Let OTF<sub>A</sub> be the 3D Fourier transform of PSF<sub>A</sub>:

$$\text{PSF}_A(x, y, z) = \iiint \text{OTF}_A(k_x, k_y, k_z) \times \exp[i(k_x x + k_y y + k_z z)] dk_x dk_y dk_z, \quad (1)$$

where  $x$ ,  $y$ , and  $z$  are real space coordinates and  $k_x$ ,  $k_y$ , and  $k_z$  are the corresponding Fourier space coordinates. For monochromatic light, OTF<sub>A</sub> is nonzero only on a two-dimensional (2D) surface: a spherical shell of radius  $2\pi n/\lambda$  (where  $n$  is the refractive index of the immersion medium and  $\lambda$  is the wavelength) limited by the aperture angle  $\alpha$  of the objective lens (Fig. 1).<sup>13,14</sup> For a low-NA system the 2D surface can

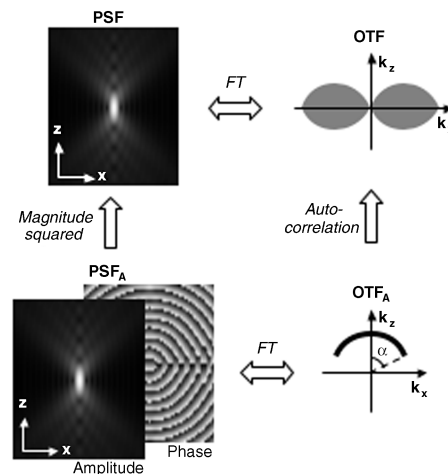


Fig. 1. Relations among four ways to characterize 3D imaging properties: FT, Fourier transform;  $\alpha$ , aperture angle; other abbreviations defined in text.

be considered flat, but in the high-NA case one must take into account the surface's spherical shape. By making axial Fourier space coordinate  $k_z$  a function of lateral coordinates  $k_x$  and  $k_y$ :

$$k_z(k_x, k_y) = [(2\pi n/\lambda)^2 - (k_x^2 + k_y^2)]^{1/2}, \quad (2)$$

we can write Eq. (1) as a 2D integral over a 2D complex-valued pupil function  $P$ :

$$\text{PSA}_A(x, y, z) = \iint P(k_x, k_y) \times \exp[ik_z(k_x, k_y)z] \exp[i(k_x x + k_y y)] dk_x dk_y. \quad (3)$$

Pupil function  $P$  is nonzero on a support that corresponds to the system's aperture and effectively represents the point source's in-focus wave front at the back focal plane of the objective lens.  $P$  describes the imaging properties of the system compactly and completely, within the monochromatic scalar model of light used here.

Phase retrieval estimates the complex-valued pupil function  $P$ —and thus the phase of the  $\text{PSF}_A$ —from measured intensity PSF. It is possible to estimate the unknown phase information because of the redundancy provided by the multiple focus levels in the measured PSF and because of *a priori* knowledge of wavelength and NA, which place geometric constraints on the pupil function.

Our method uses a modified version of the Gerchberg–Saxton algorithm<sup>15</sup> as follows: From the current estimate of the pupil function, estimated  $\text{PSF}_A$  sections were calculated with Eq. (3) (implemented as a 2D fast Fourier transform) for several values of the defocus  $z$ ; the  $\text{PSF}_A$  amplitudes were set pointwise equal to the square root of the corresponding sections of the measured intensity PSF; we then retransformed each section into a candidate pupil function by reversing Eq. (3) and discarded the values outside the known aperture. The average of these candidate pupil functions formed the updated pupil function for use in the next iteration. Unlike in the original Gerchberg–Saxton algorithm, we allow the pupil function's magnitude to vary over the aperture, as one cannot generally assume that the pupil function's magnitude is constant over the pupil for high-NA systems. For instance, high-angle rays generally suffer greater reflection losses and are more subject to polarization effects. The redundancy of the multiple focus levels compensates for the weakened Fourier space amplitude constraint.

We applied our modified phase retrieval approach to wide-field fluorescence microscopy at high NA. Red 0.12- $\mu\text{m}$ -diameter fluorescent beads<sup>11</sup> (Fluospheres, Molecular Probes) were diluted in ethanol, air dried onto a cover slip, and mounted in water. The beads were illuminated by a mercury arc lamp and imaged with a 100 $\times$  1.3-NA Zeiss Axiomat plano-apochromatic objective lens onto a liquid-nitrogen-cooled CCD. The passbands of the excitation and emission filters were 570–590 and 610–670 nm, respectively. The PSF data sets were preprocessed to correct for background, illumination intensity

variations, and photobleaching. Four sections, corresponding to  $-3$ -,  $-1$ -,  $+1$ -, and  $+3$ - $\mu\text{m}$  defocus, were selected from each PSF image stack for use in the phase retrieval. Each phase retrieval was run with a wavelength of 615 nm for 25 iterations, with a Gaussian smoothing filter applied to the averaged pupil function at every fifth iteration. The mean-squared intensity error (MSE), normalized by the summed intensity of the measured data, was used as a measure of phase-retrieval quality. For  $512 \times 512$  pixel sections the phase retrieval takes approximately 40 s on a 600-MHz, EV67 Alpha processor. Figure 2 shows amplitude and phase of three phase-retrieved pupil functions for this microscope. Both the amplitude and the phase components of the phase-retrieved pupil function are quite similar for different PSFs collected on the same optical system. The small differences, mostly in the amplitude, may be attributable to different signal-to-noise levels in the raw data, variations in the exact centering of the fluorescent bead with respect to the pixilated image, and the fact that the bead used to measure the PSF has a finite and slightly variable size. The MSE value for each of the pupils rapidly improved during the first four iterations, then more slowly; final MSE values were 0.030, 0.039, and 0.036 for the top, middle, and bottom pupils, respectively. By comparison, phase retrieval on a noise-free, simulated PSF reached a final MSE of  $7.3 \times 10^{-6}$ , whereas simulated data that contained Poisson and readout noise, at levels comparable to

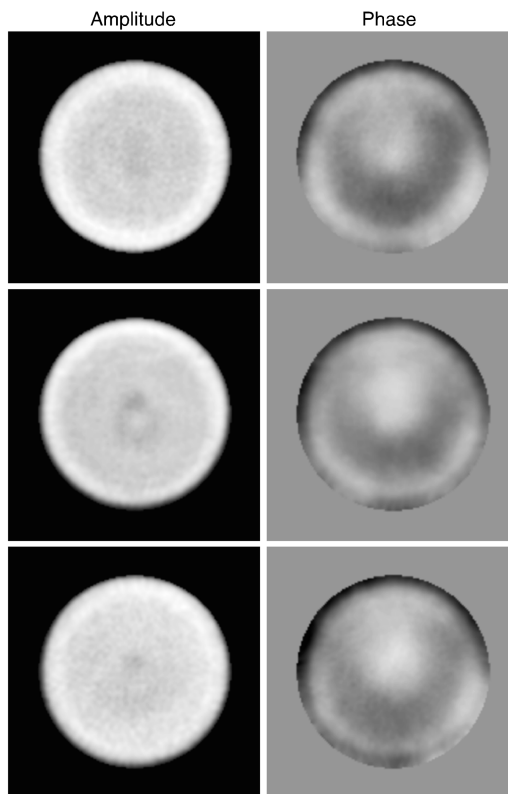


Fig. 2. Phase-retrieved pupil functions based on three different measured PSFs from the same optical system. The gray-scale range is zero to maximum amplitude, and  $-\pi/2$  to  $\pi/2$  rad for the phase.

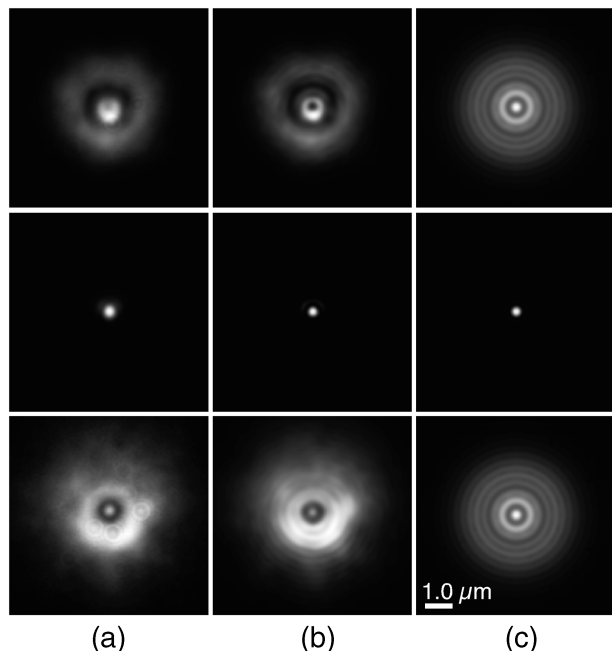


Fig. 3. Planar ( $XY$ ) sections of (a) the measured PSF, (b) a PSF calculated from the central phase-retrieved pupil function in Fig. 2, and (c) a theoretically calculated PSF. The defocus is  $-2 \mu\text{m}$ ,  $0 \mu\text{m}$ , and  $+2 \mu\text{m}$  for the top, center, and bottom rows, respectively. The gray scale ranges between the minimum and the maximum of each image individually.

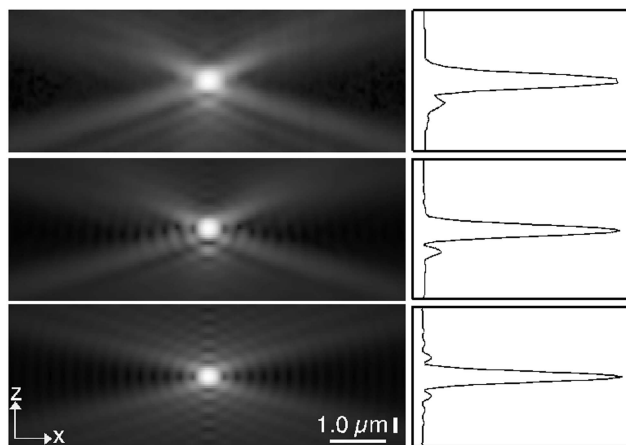


Fig. 4. Axial ( $XY$ ) sections comparing (top) measured, (middle) phase-retrieved, and (bottom) ideal PSFs. The image scaling is nonlinear to make the weak PSF features visible.

those of the lowest-signal-to-noise measured data, produced a MSE of 0.0092.

For Figs. 3 and 4 the central pupil function in Fig. 2 was used to reconstruct a phase-retrieved PSF. Compared to a theoretical, ideal PSF, which contains no lens-specific information, the phase-retrieved PSF reproduces the features of the measured PSF significantly better. The measured PSF in

Fig. 3(a) shows the considerable radial asymmetry that often occurs in microscope objective lenses; these features are well reproduced in the phase-retrieved PSF [Fig. 3(b)] but of course not in the ideal PSF [Fig. 3(c)]. Axial asymmetries are also well reproduced (Fig. 4).

Although the simplified optical model used in this Letter is able to reproduce most features of measured PSFs, a number of refinements could be made. For example, a polychromatic model<sup>10</sup> could be adopted to take into account the 20–50-nm emission bandwidth that is typical of fluorescent specimens. Similarly, the scalar light model used could be modified to take into account the vectorial nature of the electromagnetic field, as these effects are significant at high aperture angles.<sup>16</sup> Each of these corrections would tend to smooth the sharper features in the phase-retrieved, calculate PSF, improving the match with the slightly more blurred features of the measured PSF. To suppress noise, pupil functions could be expressed with a parametric model, such as a finite basis of Zernike polynomials, either after or during the iterative solution process.

This research was supported by National Institutes of Health grant GM-2510-24 to J. W. Sedat. B. M. Hanser acknowledges support from the Julius R. and Patricia A. Krevins, Lloyd M. Kozloff Fellowship, University of California, San Francisco. D. A. Agard is a Howard Hughes Medical Institute Investigator. J. W. Sedat's e-mail address is sedat@msg.ucsf.edu.

## References

1. R. A. Gonsalves, *Opt. Eng.* **21**, 829 (1982).
2. R. G. Lyon, J. E. Dorband, and J. M. Hollis, *Appl. Opt.* **36**, 1752 (1997).
3. J. H. Seldin and J. R. Fienup, *J. Opt. Soc. Am. A* **7**, 428 (1990).
4. R. G. Paxman and J. R. Fienup, *J. Opt. Soc. Am. A* **5**, 914 (1988).
5. B. A. Scalettar, J. R. Swedlow, J. W. Sedat, and D. A. Agard, *J. Microsc.* **182**, 50 (1996).
6. Z. Kam, B. Hanser, M. G. L. Gustafsson, D. A. Agard, and J. W. Sedat, *Proc. Natl. Acad. Sci. USA* **98**, 3790 (2001).
7. M. A. A. Neil, M. J. Booth, and T. Wilson, *Opt. Lett.* **23**, 1849 (1998).
8. J. R. Fienup, *Appl. Opt.* **21**, 2758 (1982).
9. D. R. Luke, J. V. Burke, and R. G. Lyon, *SIAM Rev.* **44**, 169 (2002).
10. J. R. Fienup, *J. Opt. Soc. Am. A* **16**, 1831 (1999).
11. Y. Hiraoka, J. W. Sedat, and D. A. Agard, *Biophys. J.* **57**, 325–333 (1990).
12. D. A. Agard, Y. Hiraoka, P. Shaw, and J. W. Sedat, *Methods Cell Biol.* **30**, 44 (1989).
13. C. W. McCutchen, *J. Opt. Soc. Am.* **54**, 240 (1964).
14. J. Philip, *J. Mod. Opt.* **46**, 1031 (1999).
15. R. W. Gerchberg and W. O. Saxton, *Optik (Stuttgart)* **35**, 237 (1972).
16. C. J. R. Sheppard and P. Torok, *J. Microsc.* **185**, 366 (1997).